Geophysical Research Letters

RESEARCH LETTER
10.1029/2018GL078207

Key Points:
- Damage onset depends only on the level of differential stress in any direction and so occurs at the same point regardless of the direction that σ_1 is applied
- However, the magnitude of damage also depends on the level of σ_2 in any direction, and so materials that are cyclically stressed may exhibit different damage levels in different directions
- Damage states not only depend on the individual stress state but also on the stress history

Supporting Information:
- Supporting Information S1

Correspondence to:
J. Browning,
j.browning@ucl.ac.uk

Citation:
Browning, J., Meredith, P. G., Stuart, C., Harland, S., Healy, D., & Mitchell, T. M. (2018). A directional crack damage memory effect in sandstone under true triaxial loading. *Geophysical Research Letters*, *45*, 6878–6886. https://doi.org/10.1029/2018GL078207

Received 12 APR 2018
Accepted 22 JUN 2018
Accepted article online 2 JUL 2018
Published online 20 JUL 2018

A Directional Crack Damage Memory Effect in Sandstone Under True Triaxial Loading

John Browning[1], Philip G. Meredith[1], Christopher Stuart[1], Sophie Harland[2], David Healy[2], and Thomas M. Mitchell[1]

[1]Department of Earth Sciences, University College London, London, UK, [2]School of Geosciences, University of Aberdeen, Aberdeen, UK

Abstract Crack damage leading to failure in rocks can be accumulated through cyclic stressing in the crust. However, the vast majority of experimental studies to investigate cyclic stressing apply conventional triaxial stress states ($\sigma_1 > \sigma_2 = \sigma_3$), while in nature the state of stress in the crust is generally truly triaxial ($\sigma_1 > \sigma_2 > \sigma_3$). Furthermore, the magnitude of these crustal stresses can vary over time and their orientations can also rotate over time, generating multiple crack populations and bulk anisotropic crack damage. We investigate the evolution of crack damage under both conventional and true triaxial stress conditions by sequentially and cyclically varying stresses in all three principal directions on cubic samples of dry sandstone using independently controlled stress paths. We have measured, simultaneously with stress, the bulk acoustic emission output, as a proxy for crack damage. We report a directionally controlled crack damage memory effect which has implications for the approach to failure in complex tectonic stress environments.

Plain Language Summary Fractures that lead to failure and faulting in rocks accumulate over time with increasing amounts of stress. While a considerable amount of research has been devoted to understanding how cyclic stresses lead to the development of crack damage, very little work has considered how this damage evolves with direction. The lack of work on this topic is partly due to the type of experimental apparatus required to conduct suitable tests. In order to replicate multiple populations of crack damage in different directions, a true triaxial loading apparatus is needed. Such an apparatus replicates the general state of stress in the crust and allows those stresses to be varied with direction. It is well known that the stress field around fault zones, in volcanoes, and in geothermal systems can be complex and can rotate over time. By conducting experiments using a novel true triaxial apparatus we find a directionally controlled crack damage memory effect which has implications for the approach to failure of critically stressed rocks in complex tectonic stress environments. As such, these experimental results will be of interest to those studying fault zones and volcanic processes.

1. Introduction

Rocks in the crust may undergo, or have undergone, repeated cycles of stress over time (Heap, Vinciguerra, and Meredith, 2009). In environments with complex stress regimes where stresses may evolve both spatially and temporally, such as volcanoes or active fault zones, some of these rocks may experience not only cyclic stressing but also rotating and/or reorienting stress conditions (Faulkner et al., 2006; Karaoglu et al., 2016; Gudmundsson & Philipp, 2006). In such situations the resulting crack distributions form sequentially and may therefore be highly anisotropic. Thus, the tectonic history of the crust may include complex stress paths, encompassing different magnitudes and orientations. Despite this, the way in which such variations in principal stress influence the activation and linkage of anisotropic crack distributions remains poorly constrained.

Nevertheless, stress cyclicity has been studied both in the laboratory (e.g., Browning et al., 2017; Heap et al., 2010; Holcomb, 1993; Lavrov, 2003; Lockner, 1993) and in the field (e.g., Heimisson et al., 2015; Kilburn, 2012). One well-reported phenomenon exhibited by cyclically stressed crustal rocks is the *Kaiser stress memory* effect (e.g., Holcomb, 1993; Lavrov, 2003). This effect is reported as a manifestation of materials to accumulate and reproduce information about previously experienced stress states (Lavrov, 2003). In the laboratory the effect has been observed during cyclic stressing experiments, where acoustic emission (AE) output on any cycle does not commence until the maximum stress on the previous cycle has been reached or exceeded (Heap et al., 2010; Holcomb & Costin, 1986; Lockner, 1993). All of these tests were conducted using uniaxial or conventional triaxial apparatus and so were unable to fully probe the directionality of the Kaiser effect.

More recently, Browning et al. (2017) confirmed the presence of the Kaiser effect during true triaxial stressing experiments but concluded that the effect is more accurately a *damage memory* rather than a *stress memory* effect. In general, the state of stress in the crust is triaxial (i.e., $\sigma_1 > \sigma_2 > \sigma_3$; Zoback & Zoback, 2002), and results from experiments that recreate these more realistic stress conditions have noted significant effects on rock strength (Haimson & Chang, 2000), crack densities, crack orientations (Browning et al., 2017; Ghaffari et al., 2014), and fluid flow characteristics (Nasseri et al., 2014). A Kaiser effect has also been observed at active volcanoes that are subject to cyclic deformation. The rate of seismic energy release on any deformation cycle has been found to increase only when a previous maximum stress state has been reached or exceeded (Heimisson et al., 2015; Kilburn, 2012). The implication of this, in terms of forecasting potential volcanic eruptions, is that these observed increases in seismicity may commence at stress levels closer to the critical failure stress than may have been expected. However, the question remains as to whether rocks possess a directional damage memory when they are exposed to cyclic and rotated triaxial stresses.

While Browning et al. (2017) reported a damage memory effect under true triaxial conditions, the stress orientations remained constant in their experiments. Here, therefore, we report results from an experimental study in which we measured the output of AE during conventional and true triaxial experiments on sandstone samples that have been sequentially deformed both to progressively increasing levels of stress and in multiple directions. As such, this new study represents the first experimental examination of the Kaiser effect under rotational stressing conditions.

2. Experimental Setup

The rock chosen for this study was the well-studied and well-characterized Darley Dale sandstone which is a feldspathic sandstone with a porosity of ~13%; composed of both pores and cracks (Heap, Baud, et al., 2009; Wu et al., 2000). All the results presented are from experiments performed at room temperature on dry cubic samples. Samples were manufactured with edge lengths of 50 mm (±0.03 mm) and with opposing faces ground flat and parallel to within ±0.0 l mm. All experiments were performed in a three-axis stressing frame constructed of flanged steel beams based at the laboratories of Koninklijke/Shell Exploratie en Produktie Laboratorium, Rijswijk, the Netherlands (Stuart, 1992; Stuart et al., 1993). A detailed description of the apparatus has recently been presented in Browning et al. (2017) and can also be found in the supporting information (Text S1 and Figure S2).

3. Experimental Protocol

In order to probe the level and directionality of the Kaiser effect, we have conducted three sets of experiments of progressively increasing complexity: sequential conventional triaxial (SCT) loading tests, cyclic sequential conventional triaxial (CSCT) loading tests, and cyclic sequential true triaxial (CSTT) loading tests. We present detailed results of representative experiments from each of the three sets. Overall, a total of 13 experiments were performed and a table listing the experimental conditions is given in the supporting information (Table S6).

The SCT loading tests each consisted of three loading cycles (Figure 1a). In the first cycle, σ_{zz} was increased at a rate of 0.018 MPa/s to a maximum value of 80 MPa and then unloaded at the same rate, while σ_{xx} and σ_{yy} were held constant at 4 MPa. In the second cycle, σ_{xx} was increased to 80 MPa at the same rate and then unloaded, while σ_{zz} and σ_{yy} were held constant. In the third and final cycle, σ_{yy} was loaded to 80 MPa and unloaded, while σ_{zz} and σ_{xx} were held constant.

In the subsequent CSCT test series, the applied stresses were varied both cyclically and sequentially in order to investigate the Kaiser effect (Holcomb & Costin, 1986; Lavrov, 2003; Lockner, 1993). These tests were performed by loading a sample to increasingly elevated peak stress levels in each direction sequentially (Figure 2a). In the first stage of these tests, σ_{xx} and σ_{yy} were again maintained equal at 4 MPa, while σ_{zz} was again increased to 80 MPa ($\sigma_1 > \sigma_2 = \sigma_3$). Following unloading, σ_{zz} was again increased but to a higher level than previously reached. This pattern of loading was repeated sequentially in the other two loading directions but with the maximum load in the initial loading cycle stepped down by 10 MPa for each loading direction, respectively.

Loading was again performed at a rate of 0.018 MPa/s, but unloading was rapid. This was simply for practical reasons so as to allow each test to be conducted during a single working day. Typical total experiment duration for both the SCT and CSCT tests was approximately 7 hr.

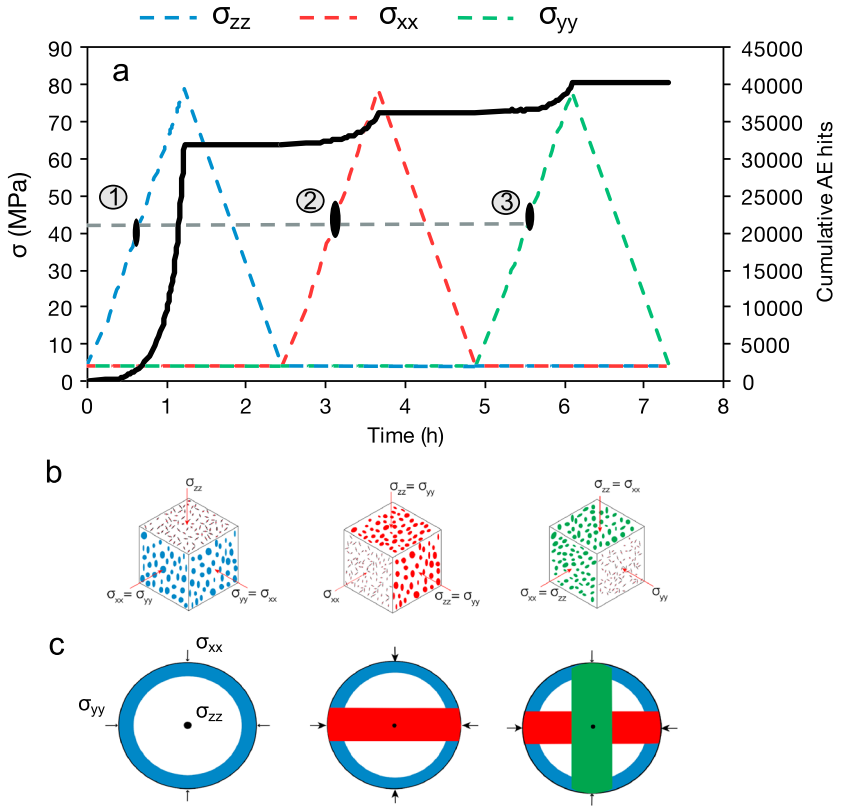

Figure 1. (a) Sequential conventional triaxial loading where σ_{zz} is first raised to 80 MPa and unloaded, followed in sequence by an identical loading pattern in the σ_{xx} and σ_{yy} directions. Cumulative AE is denoted by a black line, and the onset of AE observed in each cycle is denoted by a black ellipse. (b) Schematics showing the distribution of crack damage formed during each sequential loading cycle and (c) stereographic projections showing poles to crack planes. AE = acoustic emission.

In the final series of tests, the CSTT tests, a truly triaxial stress state was applied: $\sigma_1 > \sigma_2 > \sigma_3$. The applied stresses were varied both cyclically and in sequential directions (Figures 3a, 3c, and 3e).

In the first cycle, σ_1 was raised to 80 MPa at a rate of 0.018 MPa/s, while σ_2 was raised to 40 MPa at half that loading rate (0.009 MPa/s). In cycle 2, σ_1 and σ_2 were raised to higher stresses of 90 and 45 MPa, respectively, but at the same loading rates. In cycle 3, σ_1 was raised to a lower stress level of 60 MPa, again at the same rate, while both σ_2 and σ_3 were held constant at 4 MPa (thus applying a state of conventional triaxial stress). In cycle 4, a state of true triaxial stress was reimposed, with σ_1 being raised to 100 MPa, while σ_2 was raised to 50 MPa. In the fifth and final cycle of this sequence, a state of conventional triaxial stress was again imposed, with σ_1 being raised to 80 MPa, while σ_2 and σ_3 were both held constant at 4 MPa. After each loading cycle, the sample was unloaded to the hydrostatic state of 4 MPa in all directions. This pattern of five sequential loadings was repeated three times, first with σ_1 in the σ_{zz} direction and σ_3 in the σ_{yy} direction (cycles 1 to 5 in Figure 3a), next with σ_1 in the σ_{xx} direction and σ_3 in the σ_{zz} direction (cycles 6 to 10 in Figure 3c), and finally with σ_1 in the σ_{yy} direction and σ_3 in the σ_{xx} direction (cycles 11 to 15 in Figure 3e). As such, a total of 15 loading cycles were applied; five in each of the three loading directions.

4. Results and Discussion

4.1. SCT Loading

In the SCT loading test the AE output, which we take to mark the onset of new crack damage, commences at around 42 MPa in each of the three cycles (1, 2, and 3 in Figure 1). The AE onsets are marked as black ellipses, where the size of the ellipse indicates the picking error associated with each onset point. The onset points are shown here plotted with the cumulative AE data curves because our primary interests are damage onset and damage accumulation. However, for maximum accuracy, the onsets were actually picked from the AE rate

data curves. For completeness, therefore, all the AE rate data curves are given in the supporting information (Figures S3–S5). Figure 1 shows that the onset of new crack damage occurs at approximately the same level of stress in each cycle in the SCT test (42 ± 5 MPa), and we therefore observe absolutely no manifestation of the Kaiser effect in this experiment. However, while the AE onsets occur at approximately the same level of stress in each cycle, the level of AE output, measured as cumulative AE hits, decreases with each sequential loading cycle. In the first cycle the total number of recorded AE hits was around 32,000, whereas just 4,000 AE hits where recorded in both the second and third cycles. When taken together these results suggest that loading in the σ_{zz} generated a greater amount of crack damage than loading in the σ_{xx} and σ_{yy} directions combined, which together produced a similar level of crack damage.

As noted by Browning et al. (2017), each individual loading cycle produces a separate, cylindrically transverse isotropic (CTI) crack damage population, where cracks grow in orientations preferentially parallel to σ_1 and open normal to σ_2 and σ_3. This observation has previously been confirmed from measurement of ultrasonic wave velocities in multiple orientations using the same rock type and apparatus (Browning et al., 2017). Briefly, V_p (primary wave velocities) are found to increase in the direction normal to σ_1 during loading due to elastic crack closure and decrease during unloading, due to elastic crack opening. V_p normal to σ_2 and σ_3 (which are equal) are found to decrease at the onset crack damage formation, which was also found to be around 42 MPa, suggesting that those inelastic crack populations open normal to $\sigma_2 = \sigma_3$. V_p in these orientations do not recover following unloading, indicating the formation of new crack damage. As the onset of AE occurs at around 42 MPa in the SCT test we take this to indicate that a new population of cracks, each with CTI, are formed in each sequential cycle. The schematic diagrams in Figure 1b indicate the orientation of the *new* crack damage in each sequential cycle.

This crack damage can also be represented as poles to crack planes on a stereographic projection (Figure 1c). In the first of the three cycles, once a differential stress ($\Delta\sigma$) of 36 MPa has been reached, cracks form essentially parallel to σ_{zz} and open essentially perpendicular to σ_{xx} and σ_{yy} and so are drawn as a colored girdle of poles in the *x-y* plane. The breadth of the girdle is represented as 36° since it has previously been recognized that all fractures in the population do not form perfectly parallel to σ_1 but over a range of angles of about ±18° either side of σ_1 (see Browning et al., 2017). In the subsequent cycle, cracks form parallel to σ_{xx} and open perpendicular to σ_{zz} and σ_{yy}, so this damage is represented as a girdle in the *z-y* plane (with the same width of 36°) but is additional to the *previous* damage in the *x-y* plane which remains. When the damage from the third and final cycle is added (Figure 1c), the resulting stereogram displays only small sectors of *undamaged* space, so that the three individual anisotropic crack populations combine to produce an essentially isotropically damaged rock volume.

The range of crack angles represented in the girdles is also consistent with the measurement of significantly fewer AE hits on the second and third loading cycles. Since many of the cracks that would have been nucleated in these later cycles if the alignment was perfect have already been nucleated on previous cycles, these cracks do not need to be nucleated again; hence, the AE count is lower in later cycles.

4.2. CSCT Loading

In the first cycle (cycle 1) of the CSCT test, the sample was loaded at a constant rate to a peak stress of 75 MPa in the σ_{zz} direction, while σ_{xx} and σ_{yy} were held constant at 4 MPa (blue lines in Figure 2a). The σ_{zz} was then decreased, and the sample returned to a hydrostatic stress state of 4 MPa. In cycle 2, σ_{zz} was increased to a higher peak stress of 81 MPa, while σ_{xx} and σ_{yy} were again held constant at 4 MPa. The onset of AE in the first cycle commenced around 40 MPa, and AE output increased quasi-exponentially with increased loading, until a total of around 22,000 AE hits were recorded by the peak stress. In the second cycle, further AE only recommenced at a level of stress that was significantly higher than the onset stress on the first cycle and close to, but lower than, the previous maximum stress. This demonstrates a Kaiser effect, albeit an imperfect one. This occurrence of an AE onset at a stress level somewhat below the previous maximum is a common observation in cyclic loading experiments and occurs because the new crack damage lags behind the level of stress imposed during the relatively rapid and continuous loading applied in the laboratory (e.g., Heap et al., 2010; Lavrov, 2001). Hence, new damage (and associated AE) commences when the previous damage state is reached, rather than the previous stress state. This observation serves to support our contention that the Kaiser effect is a damage memory rather than a stress memory effect. Once it has recommenced, the AE

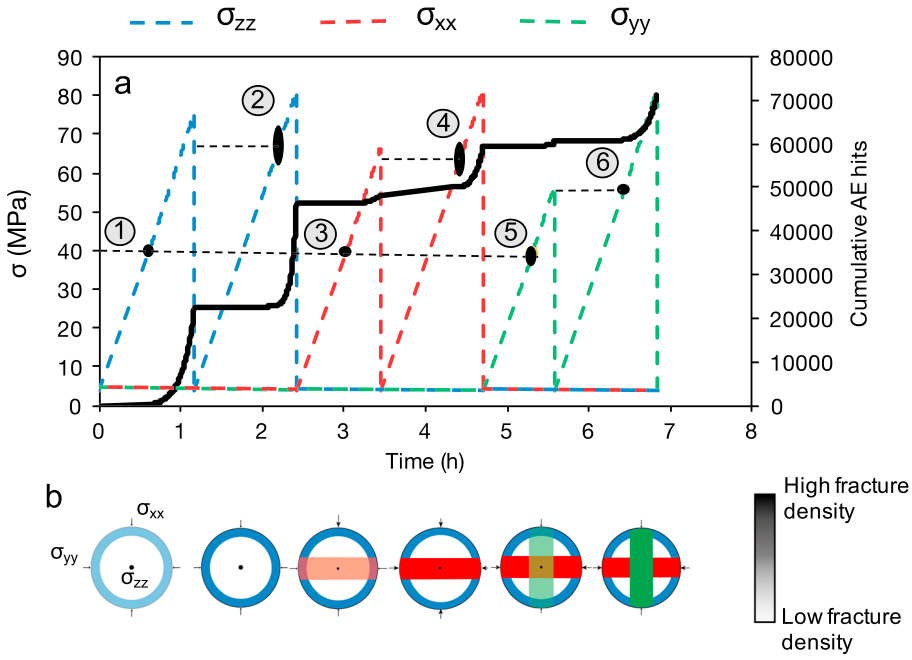

Figure 2. Cyclic sequential conventional triaxial loading where σ_{zz} is raised to 75 MPa and then unloaded and raised higher to 80 MPa. The σ_{xx} is raised to 65 and 80 MPa, and σ_{yy} is raised to 55 and 80 MPa. Cumulative AE is denoted by the solid black line, and the onset of AE observed in each cycle is denoted by a black ellipse. (b) Stereographic projections of crack damage formed during each sequential loading cycle, with increasing crack density represented by increasing color intensity. AE = acoustic emission.

again increased quasi-exponentially with increased loading; with a cumulative count of around 45,000 hits by the time the maximum stress of 81 MPa was reached.

This pattern of cyclic loading was then repeated but with the maximum load now applied in the σ_{xx} direction (red lines in Figure 2a). In cycle 3, σ_{xx} was increased to a peak value of 65 MPa, 10 MPa lower than the peak stress in cycle 1, with $\sigma_{zz} = \sigma_{yy} = 4$ MPa. However, even though this peak stress in the σ_{xx} direction was lower than either of those in cycles 1 and 2, significant AE was generated. The onset of AE again occurred at around 40 MPa, but significantly fewer AE hits were generated. This indicates the presence of new crack damage, albeit much less than in the previous cycles. Following unloading, σ_{xx} was raised to a peak stress of 80 MPa in cycle 4. Again, AE recommenced at a level of stress that was slightly lower than the previous maximum stress but significantly higher than the onset stress in cycle 3. AE output accelerated with increasing stress until unloading, generating around 10,000 hits. As we observe an onset of AE at around 40 MPa in both cycles 1 and 3, this shows no manifestation of the Kaiser effect but instead indicates a directional independence. This interpretation is supported by the observation that the Kaiser effect is restored in cycle 4.

In the final set of sequential cycles, σ_{yy} was loaded to 55 MPa in cycle 5, again 10 MPa lower than in cycle 3 and 20 MPa lower than in cycle 1 (green lines in Figure 2a). Despite this, we observe exactly the same set of phenomena; AE output again commenced around 40 MPa and accelerated with increasing stress but with significantly fewer hits than in either of cycles 1 or 3. On the final cycle (cycle 6), σ_{yy} was raised to 80 MPa. AE on this cycle recommenced at almost exactly the previous maximum stress level in cycle 5 and increased up to the peak stress, generating a similar number of AE hits to cycle 4.

The AE results from these CSCT tests highlight that the Kaiser effect is in fact a damage-memory effect where new crack damage is only initiated when the previous damage state is exceeded. We can again highlight the evolution of crack damage during CSCT loading using stereographic projections of poles to crack planes (Figure 2b), but we now have to consider the sequential increase in density of each crack population as well as their orientations. We qualitatively estimate the contemporaneous change in crack density from the quantitative output of AE hits recorded during each loading cycle. The maximum stress is decreased in each of the

initial loading cycles (1, 3, and 5), and so the amount of crack damage generated during each of these cycles also decreases. In the second set of loading cycles (2, 4, and 6), the sample is loaded to the same maximum stress (80 MPa) in each direction, and so the final crack densities are expected to mimic those generated in the SCT test (Figure 1b). We represented increases in crack density by increases in color intensity in the stereograms of Figure 2b.

4.3. CSTT Loading

The results and observations from all 15 cycles of one of our CSTT test are described and summarized below and illustrated in Figure 3:

Cycles 1–5 (Figures 3a and 3b)

- AE onset in cycle 1 occurs when σ_{zz} reaches around 40 MPa. The total number of AE hits generated during loading to the peak stress of 80 MPa was around 6,600. This contrasts with the 32,000 hits generated during loading to the same peak stress in the first cycle of the SCT test (Figure 3a). Since the stress regime in this cycle is truly triaxial, the crack damage population is characterized by planar transverse isotropy (PTI) with cracks restricted to grow subparallel to σ_1 (σ_{zz}) and subnormal to σ_3 (σ_{yy}), rather than the CTI characteristic of conventional triaxial loading in the SCT test where cracks were able to grow in any orientation in the σ_1-σ_3 plane, as previously shown by Browning et al. (2017). As such, the poles to crack planes are plotted as small circles of ±18° centered on the σ_{yy} axis (Figure 3b), rather than as a girdle around the *x*-*y* plane (as in Figure 1b). The decrease in AE output recorded in the CSTT test, relative to the SCT test, is entirely commensurate with the restricted range of crack orientations.
- In cycle 2, AE output recommence only when σ_{zz} reaches 80 MPa. This is a manifestation of the Kaiser effect; new damage (and, hence, new AE) is only generated when the maximum stress in the previous cycle (cycle 1) is exceeded. Cycle 2 is also truly triaxial, meaning that new crack damage is also characterized by PTI. Hence, the stereogram for this cycle is also plotted as small circles around the σ_{yy} axis (Figure 3b) but with increased color intensity to indicate the higher crack density.
- A very different pattern of activity is observed in cycle 3 where the sample is subjected to conventional triaxial loading ($\sigma_{xx} = \sigma_{yy}$). AE output recommences when σ_{zz} reaches 40 MPa, a much lower stress level than in cycle 2 but the same level as for the AE onset in cycle 1. This is because cracks around the *x*-*y* plane that were suppressed from growing in the first two cycles due to the elevated level of the intermediate stress (σ_{xx}) are now able to grow. We now have CTI conditions under a conventional triaxial stress regime, and the stereogram for this cycle is therefore plotted as a girdle around the *x*-*y* plane (Figure 3b) but with low color intensity to indicate the relatively low density of the infilling cracks; only about 2,000 AE hits were generated during this loading cycle. We again note that the concept of the Kaiser effect as a simple stress memory effect also breaks down here. The onset of new AE occurred not at the previous maximum stress level (90 MPa) but at the overall stress state where it became possible for new, oriented crack damage to be generated.
- In cycle 4, we again impose true triaxial loading and AE recommences, as expected, at the point where the maximum stress in cycle 2 (90 MPa) is exceeded, rather than at the maximum stress in cycle 3 (65 MPa). So a restoration of the directional aspect of the Kaiser effect is observed in this cycle. Because of the imposed true triaxial loading, crack damage is again restricted to PTI, so the stereogram is plotted as small circles around the σ_{yy} axis (Figure 3b), with increased color intensity to represent the increased crack density.
- In cycle 5 we revert back to conventional triaxial loading. AE output recommences at the previous maximum stress level in cycle 3 (65 MPa), rather than the higher maximum stress level of 100 MPa in cycle 4. So while the concept of the Kaiser effect as a simple stress memory effect broke down between cycles 2 and 3, its directional aspect is restored between cycles 3 and 5. New crack damage again exhibits CTI, so the stereogram for cycle 5 is a girdle around the *x*-*y* plane with increased color intensity.
- The total cumulative number of AE hits generated during loading cycles 1–5 was approximately 30,000 (Figure 3a).

Cycles 6–10 (Figures 3c and 3d)

- The sequence of loading and the pattern of AE activity and onset during loading cycles 6–10 were essentially identical to those during cycles 1–5 but with σ_{xx} as σ_1 and σ_{zz} as σ_3 (Figure 3c).

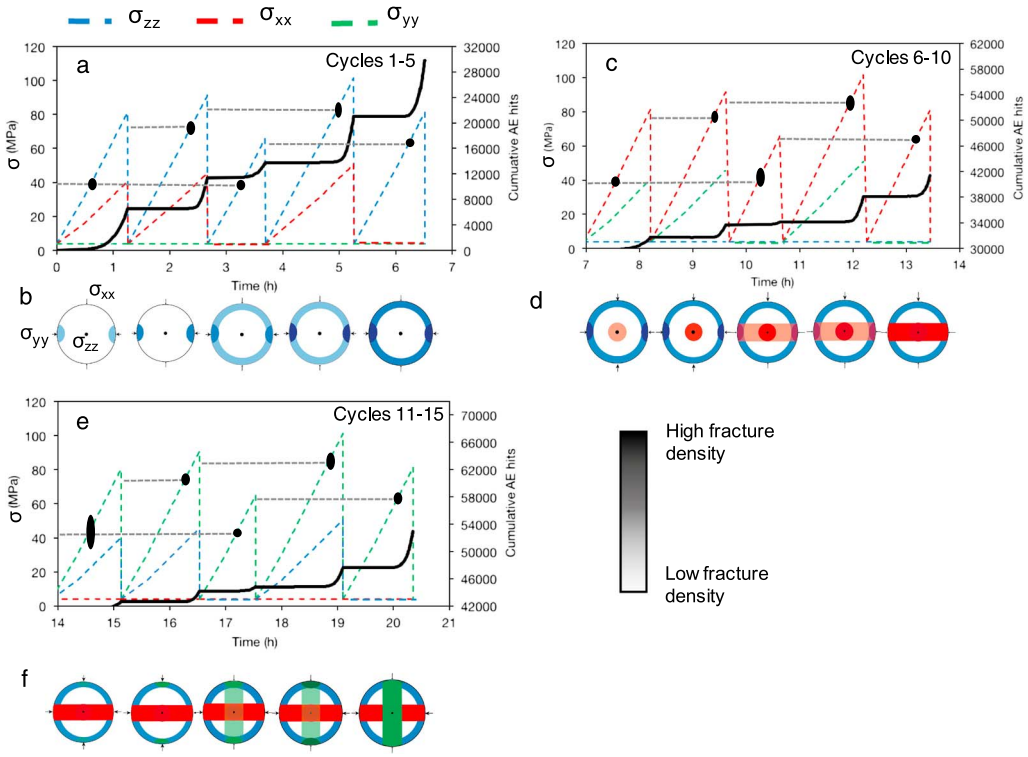

Figure 3. Cyclic sequential true triaxial loading test. (a) Cycles 1–5 with corresponding crack damage stereonets (b), (c and d) cycles 6–10, and (e and f) cycles 11–15. AE = acoustic emission.

- Just as for cycles 1 and 3, we observe AE onsets around 40 MPa in cycles 6 and 8. In cycle 7, we observe an AE onset a little below 80 MPa (as for cycle 2). In cycle 9, the AE onset occurs a little below 90 MPa (as for cycle 4), and finally in cycle 10 the AE onset occurs around 65 MPa (as for cycle 5).
- We show in Figure 3b how crack damage generated in loading cycles 1–5 could be represented graphically as stereograms. These stereograms also serve to illustrate how the crack damage induced in each cycle is additive. The damage stereograms for cycles 6–10 are shown in Figure 3d. They follow the same pattern as those for cycles 1–5, but true triaxial damage is shown as small circles centered on the σ_{zz} axis, and conventional triaxial damage is shown as girdles around the *y-z* plane. However, the stereograms of Figure 3d show that not only is the damage induced in cycles 6–10 internally additive but it is also additive to the damage population induced in cycles 1–5.
- We note that the total cumulative number of AE hits generated during loading cycles 6–10 was approximately 12,000 (Figure 3c), about 40% of the number generated during cycles 1–5. This is as expected because a significant number of the cracks that would be expected to grow in particular orientations during loading cycles 6–10 have already been propagated (and generated AE signals) during cycles 1–5. Since those cracks already exist, they do not generate AE on subsequent loading.

Cycles 11–15 (Figures 3e and 3f)

- The sequence of loading and the pattern of AE activity and onset during loading cycles 11–15 were again essentially identical to those during cycles 1–5 and 6–10 but with σ_{yy} as σ_1 and σ_{xx} as σ_3 (Figure 3e).
- Again, the pattern of AE onsets in cycles 11–15 is identical to those in cycles 1–5 and 6–10.
- The stereograms of crack damage for cycles 11–15 (Figure 3f) also follow the same pattern as those for cycles 1–5 and 6–10 but with true triaxial damage shown as small circles centered on the σ_{xx} axis and conventional triaxial damage shown as girdles around the *z-x* plane. Once again, the stereograms of Figure 3f show that the crack damage induced during cycles 11–15 is not only internally additive but also additive to the damage populations induced in cycles 1–5 and 6–10.

- The total cumulative number of AE hits generated during loading cycles 11–15 was again approximately 12,000 (Figure 3e), the same as the number generated during cycles 6–10 and 40% of the number generated during cycles 1–5. This is entirely as expected for the same reasons as noted above.

5. Concluding Remarks

We consider that the results presented here have fundamental implications for the approach to failure of crustal structures that have experienced complex loading paths due to variations in stress orientation and magnitude over geological time. This is because crack damage in natural crustal systems such as fault zones and volcanoes evolves in different ways depending on the stress history (Healy et al., 2015). Cyclic loading of crustal structures is common and leads to the progressive evolution of damage populations. Our results demonstrate that the onset of damage in any orientation depends only on the level of differential stress (σ_1–σ_3) in that orientation. However, the orientation and magnitude of the evolving damage also depends on the level of σ_2, because a lower level of σ_2 leads to a less restricted range of available crack orientations and, hence, to an increased number of cracks. Furthermore, the damage generated during each loading cycle is incrementally additive. Additionally, stress rotations in the crust lead to the potential for the evolution of anisotropic damage. Our results show how rotation of the principal stresses leads to the generation of directionally independent (anisotropic) damage populations. Hence, where crustal structures are subjected to both cyclical and rotational loading over geological time, multiple crack populations will be generated each exhibiting independent but directionally controlled damage memory (Kaiser) effects.

This is important because, for example, a large amount of effort has been expended in modeling the cyclic deformation and seismicity that precede volcanic eruptions (Heimisson et al., 2015; Kilburn, 2012). The rock mechanical data that have been used as input to these models have necessarily all been obtained from experiments conducted under uniaxial or conventional triaxial stress conditions, owing to their availability. However, such data are unable fully to capture the richness of how additive and directional damage populations evolve under the true triaxial conditions that pertain in the crust. We therefore suggest that models of cyclic deformation and seismicity in the crust should in future account for truly triaxial stress states and the potential for stress reorientation so that they can encompass the role of such additive and directional damage populations in the approach to crustal failure.

Furthermore, previously published work on brittle deformation under true triaxial stress conditions has often invoked the use of stress invariants in analyzing failure. Reches and Dieterich (1983) used the first and second invariants J_1 and J_2, where $J_1 = \sigma_1 + \sigma_2 + \sigma_3$ and $J_2 = \sigma_1.\sigma_2 + \sigma_2.\sigma_3 + \sigma_3.\sigma_1$, and found that failure by shear faulting occurred when $J_2 = aJ_1{}^b$, where a and b are constants for the specific rock. The analysis by Colmenares and Zoback (2002) describes other criteria that use some combination of the invariants J_1, J_2, or J_3 (= $\sigma_1.\sigma_2.\sigma_3$) to analyze failure. However, in this study we are concerned with the evolution of crack damage that precedes ultimate failure. Our findings clearly show that such damage is a distinctly directional phenomenon, especially under true triaxial stress states (Browning et al., 2017). The fundamental and intrinsic attribute of any tensor invariant, that it is identical under any geometrical transformation, only serves to conceal the significance of this specific directionality (e.g., of sequentially evolving damage populations) with respect to the principal stresses and their orientations. Furthermore, existing brittle failure criteria for true triaxial stress states do not predict the orientations of the shear failure planes. Our results therefore suggest that future work should be directed to incorporating directional damage into such failure criteria.

Acknowledgments
We thank J. G. Van Munster for providing access to the true triaxial apparatus at KSEPL and for technical support during the experimental program We are grateful for comments from the Editor Gavin Hayes, and from an anonymous reviewer and Philip Benson. This work was partly funded by NERC awards NE/N002938/1 and NE/N003063/1 and by a NERC Doctoral Studentship, which we gratefully acknowledge. Supporting information are included in an SI file; any additional data may be obtained from J. B. (email: j.browning@ucl.ac.uk).

References

Browning, J., Meredith, P. G., Stuart, C. E., Healy, D., Harland, S., & Mitchell, T. M. (2017). Acoustic characterization of crack damage evolution in sandstone deformed under conventional and true triaxial loading. *Journal of Geophysical Research: Solid Earth*, *122*, 4396–4412. https://doi.org/10.1002/2016JB013646

Colmenares, L. B., & Zoback, M. D. (2002). A statistical evaluation of intact rock failure criteria constrained by polyaxial test data for five different rocks. *International Journal of Rock Mechanics and Mining Sciences*, *39*(6), 695–729. https://doi.org/10.1016/S1365-1609(02)00048-5

Faulkner, D. R., Mitchell, T. M., Healy, D., & Heap, M. J. (2006). Slip on'weak'faults by the rotation of regional stress in the fracture damage zone. *Nature*, *444*(7121), 922.

Ghaffari, H. O., Nasseri, M. H. B., & Young, R. P. (2014). Faulting of rocks in a three dimensional stress field by micro-anticracks. *Scientific Reports*, *4*, 1–7.

Gudmundsson, A., & Philipp, S. L. (2006). How local stress fields prevent volcanic eruptions. *Journal of Volcanology and Geothermal Research*, *158*(3–4), 257–268.

Haimson, B., & Chang, C. (2000). A new true triaxial cell for testing mechanical properties of rock, and its use to determine rock strength and deformability of Westerly granite. *International Journal of Rock Mechanics and Mining Sciences*, *37*(1-2), 285–296. https://doi.org/10.1016/S1365-1609(99)00106-9

Healy, D., Blenkinsop, T. G., Timms, N. E., Meredith, P. G., Mitchell, T. M., & Cooke, M. L. (2015). Polymodal faulting: Time for a new angle on shear failure. *Journal of Structural Geology*, *80*, 57–71. https://doi.org/10.1016/j.jsg.2015.08.013

Heap, M. J., Baud, P., Meredith, P. G., Bell, A. F., & Main, I. G. (2009). Time-dependent brittle creep in Darley Dale sandstone. *Journal of Geophysical Research*, *114*, B07203. https://doi.org/10.1029/2008JB006212

Heap, M. J., Faulkner, D. R., Meredith, P. G., & Vinciguerra, S. (2010). Elastic moduli evolution and accompanying stress changes with increasing crack damage: Implications for stress changes around fault zones and volcanoes during deformation. *Geophysical Journal International*, *183*(1), 225–236.

Heap, M. J., Vinciguerra, S., & Meredith, P. G. (2009). The evolution of elastic moduli with increasing crack damage during cyclic stressing of a basalt from Mt. Etna volcano. *Tectonophysics*, *471*(1-2), 153–160. https://doi.org/10.1016/j.tecto.2008.10.004

Heimisson, E. R., Einarsson, P., Sigmundsson, F., & Brandsdóttir, B. (2015). Kilometer-scale Kaiser effect identified in Krafla volcano, Iceland. *Geophysical Research Letters*, *42*, 7958–7965. https://doi.org/10.1002/2015GL065680

Holcomb, D. J. (1993). General theory of the Kaiser effect. *International Journal of Rock Mechanics and Mining Science and Geomechanics Abstracts*, *30*(7), 929–935. https://doi.org/10.1016/0148-9062(93)90047-H

Holcomb, D. J., & Costin, L. S. (1986). Detecting damage surfaces in brittle materials using acoustic emissions. *Journal of Applied Mechanics*, *53*(3), 536.

Karaoglu, O., Browning, J., Bazargan, M., & Gudmundsson, A. (2016). Numerical modelling of triple-junction tectonics at Karliova, Eastern Turkey, with implications for regional magma transport. *Earth and Planetary Science Letters*, *452*, 157–170.

Kilburn, C. (2012). Precursory deformation and fracture before brittle rock failure and potential application to volcanic unrest. *Journal of Geophysical Research*, *117*, B02211. https://doi.org/10.1029/2011JB008703

Lavrov, A. (2001). Kaiser effect observation in brittle rock cyclically loaded with different loading rates. *Mechanics of Materials*, *33*(11), 669–677.

Lavrov, A. (2003). The Kaiser effect in rocks: Principles and stress estimation techniques. *International Journal of Rock Mechanics and Mining Sciences*, *40*(2), 151–171.

Lockner, D. (1993). The role of acoustic emission in the study of rock fracture. International loading rates. *Mechanics of Materials*, *33*(11), 669–677.

Nasseri, M. H. B., Goodfellow, S. D., Lombos, L., & Young, R. P. (2014). 3-D transport and acoustic properties of Fontainebleau sandstone during true-triaxial deformation experiments. *International Journal of RockMechanics and Mining Sciences*, *69*, 1–18.

Reches, Z. E., & Dieterich, J. H. (1983). Faulting of rocks in three-dimensional strain fields I. Failure of rocks in polyaxial, servo-control experiments. *Tectonophysics*, *95*(1–2), 111–132.

Stuart, C. E. (1992). Evolution of anisotropic microcrack damage in cyclically stressed rock, characterized by contemporaneous acoustic emission and elastic wave velocity measurements, Unpublished thesis, University of London.

Stuart, C. E., Meredith, P. G., Murrell, S. A. F., & Van Munster, J. G. (1993). Anisotropic crack damage and stress-memory effects in rocks under triaxial loading. *International Journal of Rock Mechanics and Mining Science and Geomechanics Abstracts*, *30*(7), 937–941. https://doi.org/10.1016/0148-9062(93)90048-I

Wu, X. Y., Baud, P., & Wong, T. F. (2000). Micromechanics of compressive failure and spatial evolution of anisotropic damage in Darley Dale sandstone. *International Journal of Rock Mechanics and Mining Sciences*, *37*(1–2), 143–160.

Zoback, M. D., & Zoback, M. L. (2002). State of stress in the Earth's lithosphere. *International Geophysics*, *81*, 559–XII.